The Size-Templating Matrix Effect in Vesicle Formation I: A Microscopic Model and Analysis

C. D. Bolton* and J. A. D. Wattis†

Theoretical Mechanics, School of Mathematical Sciences, University of Nottingham, University Park, Nottingham, NG7 2RD, U.K.

Received: September 3, 2002; In Final Form: February 21, 2003

Recently it has been reported that the growth of vesicles is strongly affected by the presence of preformed vesicles. In particular, the final distribution is strongly biased toward the size of the preformed vesicles. This size-templating effect is called the "matrix" effect. Turbidity measurements have revealed some characteristic features of such systems in which a fast phase of dynamics over which turbidity rises sharply is followed by a much slower phase of kinetics. Experimentally it has been observed that the larger the size of a pre-added vesicle, the higher the turbidity at the end of the fast phase and the longer this phase persists. Additionally, a system without pre-added vesicles has slower, but more sustained, dynamics. We develop a microscopic model based on a novel generalization of the Becker−Döring equations of nucleation, which describes the stepwise growth of vesicles. We assume that a preexisting vesicle provides a catalytic surface on which a vesicle fragment can grow at an accelerated rate. The model involves aggregation and fragmentation rate coefficients, which together determine an equilibrium solution. The model derived is strongly nonlinear and describes the dynamics far from the equilibrium solution. We numerically integrate the model from a variety of initial conditions and use an approximate measure of turbidity to compare our results with experiments previously performed. Comparison with the experiments show good qualitative agreement, validating the modeling assumptions made.

1. Introduction

Searching for the origins of life holds many inherent challenges: by its nature an improbable event occurring in the distant past defies direct observation. It is a staggering leap in complexity from simple structures such as amino acids, sugars, nucleic bases, and fatty acids[1] to even the most basic living cell, a process likely to contain many stages. Self-reproducing molecular systems have been investigated because they exhibit the fundamental properties of a living system. Consider a prebiotic soup containing surfactant molecules: if the concentration of surfactant exceeds the critical aggregate concentration (CAC), then remarkably, vesicles spontaneously form, driven by an increase in entropy of the surrounding water. The structure of the vesicle, a spherical lipid bilayer with an aqueous core separated from the surrounding environment, has a tantalizing analogy with a biological cell.[2] We present a microscopic mathematical model for the formation of vesicles based on a novel generalization of the Becker and Döring equations and analyze this numerically, comparing the results with experimental data.

The importance of self-reproduction and autocatalysis is demonstrated by a numerical example provided by Lifson,[7] in which he considers a process which produces one molecule of product each microsecond: to amass 1 mol of product from a single molecule takes 6×10^{23} μs, longer than the age of the universe. In contrast, if the reaction is autocatalytic and the product doubles every microsecond, 1 mol is obtained in 79 μs. Clearly then, the mechanism of such a powerful tool warrants closer examination.

Much of the work we review here is done by Luisi's group at ETH-Zentrum.[3,4,5,8−11] Walde et al.[3] used fatty acid (caprilic and oleic) vesicles to demonstrate an autopoietic self-reproductive process. This system exhibited an increase in the formation of vesicles due to a reaction within the boundary of existing vesicles; hence, the growth of vesicles was accelerated after an initial phase lag. The autocatalytic effect was confirmed by demonstrating that the phase lag is much reduced by the presence of pre-added vesicles. These experiments relied on the hydrolysis of a precursor to produce the surfactant required to construct the vesicles, and the catalytic nature arises from the fact that the vesicles themselves efficiently hydrolyze the precursor. Mavelli and Luisi[5] first proposed a simplified kinetic model of this system, and later Coveney and Wattis[6] formulated and studied a nonlinear theoretical model of the formation of vesicles from a stock of precursor.

Recent experiments have been initiated from a stock of surfactant, eliminating the reliance on the hydrolysis of a precursor. Blöchliger et al.[4] has investigated the growth of oleic acid/oleate vesicles by pre-adding vesicles with a monodisperse distribution (with mean size either 50 or 100 nm) to an initial stock of surfactant. By "monodisperse" vesicles we mean a distribution of vesicle size centered about a particular size with a very small standard deviation; this is achieved by extruding the vesicles through a polycarbonate membrane such that the size of the resulting vesicles corresponds to the size of the pores in the membrane. The growth of vesicles was observed by a combination of freeze-fracture electron microscopy and turbidity measurements. The final distribution of vesicle sizes was found to be strongly biased toward the diameter of the pre-added vesicles; this phenomenon was labeled the "matrix" effect. In contrast, without any pre-added vesicles, the final distribution was relatively polydisperse. Further work by Lonchin et al.[9] demonstrates the matrix effect for a system of oleate micelles with pre-added 1-palmitoyl-2-oleate-*sn*-glycero-3-phosphocho-

* Corresponding author. E-mail: Colin.Bolton@maths.nottingham.ac.uk.
† E-mail: Jonathan.Wattis@nottingham.ac.uk.

10.1021/jp026897z CCC: $25.00
Published on Web 06/28/2003

line (POPC) vesicles, and they claim their results are applicable to a wide range of vesicular systems. A drawback of these experiments is that it is impossible to distinguish in the final distribution the contribution from pre-added, or newly formed, vesicles. A novel experiment was pioneered by Berclaz et al.,[10] where the pre-added vesicles were "tagged" by trapping ferritin molecules inside the vesicle wall; because of the dense iron core of the ferritin molecule these can easily be detected by cryotransmission electron microscopy analysis. It was concluded that the initial monomers were mostly concentrated in new vesicles with a size which does not exceed the size of the pre-added vesicle. Berclaz et al.[11] exploited this technique to investigate the mechanism of vesicle growth in the presence of pre-added vesicles for oleic acid/oleate and POPC/oleic acid/oleate vesicles. If only de novo vesicle formation occurs, we expect to observe many untagged vesicles, as is the case with no pre-added vesicles. Alternatively, the presence of tagged pre-added vesicles may introduce a new process of vesicle formation such as splitting, growth of vesicles inside pre-added vesicles, or growth of new vesicles on the surface of pre-added vesicles. We broadly define these as fission processes. In this case, we expect the ferritin molecules to be redistributed between the vesicles formed. In fact, the latter case was found to be prevalent, so they concluded that not only did a fission process exist but also that it dominates the de novo process.

These recent advances have extended our experimental understanding of vesicle formation, and in this paper we develop a theoretical understanding of these results. In section 2, we first present the model of nucleation proposed by Becker and Döring,[12] which describes general stepwise nucleation, and then we extend this model to incorporate a fission mechanism to explain the size-templating matrix effect recently observed. We note that the model is a nonlinear description, which is valid far from equilibrium states as well as at equilibrium. We also determine the timescales of the dynamics starting from various initial conditions. We numerically solve the system in section 3, both with and without pre-added vesicles. We show that the model captures the main elements of the experiments, thus validating the modeling assumptions made. Finally, in section 4 we conclude by discussing our results.

2. Modeling

2.1. Becker−Döring Model. The Becker−Döring equations were originally formulated to describe the kinetics of nonequilibrium gas−liquid-phase transitions, where it was proposed that clusters form by the addition or subtraction of single particles (monomers) with no interaction between larger clusters. Such larger clusters evolve by maintaining a dynamic balance of monomer aggregation and fragmentation. This process is modeled as a chemical reaction, and by denoting an r-sized cluster as C_r, we have the reversible reaction

$$C_r + C_1 \rightleftharpoons C_{r+1} \tag{1}$$

For each reaction, there are two reaction rates to prescribe. We denote the forward rate by a_r and the reverse by b_{r+1}, both are nonnegative. In the original formulation the concentration of monomers was assumed constant, but later Penrose[13] generalized this model to allow the monomer concentration to vary, ensuring instead the conservation of mass:

$$\rho = \sum_{r=1}^{\infty} r c_r \tag{2}$$

This modified model is still referred to as the Becker−Döring model. The stepwise aggregation and fragmentation is the central feature of the Becker−Döring model and is an inherent assumption underlying all the following analysis. Smoluchowski[14] proposed a more general model allowing for cluster−cluster aggregation and for a cluster to split into uneven fragments; however, this is a far more complex model.

Defining J_r as the net flux from cluster size r to $r+1$ and $c_r(t)$ as the concentration of clusters C_r at time t, we express the system by

$$\dot{c}_1 = -J_1 - \sum_{r=1}^{\infty} J_r \tag{3}$$

$$\dot{c}_r = J_{r-1} - J_r, \qquad r \geq 2 \tag{4}$$

$$J_r = a_r c_1 c_r - b_{r+1} c_{r+1}, \qquad r \geq 1 \tag{5}$$

There is an alternative way of writing the infinite set of ordinary differential equations. For an arbitrary sequence of numbers $\{g_r\}_{r=1}^{\infty}$, the following identity holds:

$$\sum_{r=1}^{\infty} g_r \dot{c}_r = \sum_{r=1}^{\infty} (g_{r+1} - g_r - g_1) J_r \tag{6}$$

and this is equivalent to the original set of eqs 3 and 4.

We define Q_r, the cluster partition function, in terms of the forward and reverse reaction rates by $a_r Q_r = b_{r+1} Q_{r+1}$ and insist that $Q_1 = 1$. We define the quantity:

$$V = \sum_{r=1}^{\infty} c_r \left(\log\left(\frac{c_r}{Q_r}\right) - 1 \right) \tag{7}$$

We differentiate this function by using eq 6 with $g_r = \log(c_r/Q_r)$ to yield

$$\dot{V} = -\sum_{r=1}^{\infty} \frac{b_{r+1}}{Q_r} (\log(c_1 c_r Q_{r+1}) - \log(c_{r+1} Q_r))(Q_{r+1} c_1 c_r - c_{r+1} Q_r) \tag{8}$$

where each element of the sum has the form $P(A - B)\log(A/B)$ with $P > 0$ and hence is positive. Thus, $\dot{V} \leq 0$ with $\dot{V} = 0$ only when the system is in equilibrium. Hence, V qualifies as a Lyapunov function (and is associated with the Helmholtz free energy of the system), ensuring the system has a unique equilibrium solution, denoted by $\bar{c}_r = Q_r \bar{c}_1^r$. The partition function can be related to the chemical potential of the system. Writing the temperature as T and Boltzmann's constant as k, we denote the chemical potential for a vesicle of size r as

$$\mu_r = \mu_r^{\Theta} + kT \log c_r \tag{9}$$

where μ_r^{Θ} is the standard-state potential of a cluster of size r. If we set the standard chemical potential of monomers to zero (that is, $\mu_1^{\Theta} = 0$), then the condition of thermodynamic equilibrium $\mu_r = r\mu_1$ implies

$$\mu_r^{\Theta} = -kT \log Q_r \tag{10}$$

and thus we link the partition function with the chemical potential. Alternatively, Q_r can be thought of as a global equilibrium constant.

The asymptotic solution for size-independent aggregation and fragmentation rates has been described by King and Wattis.[15] Such is the rich structure of the Becker−Döring equations that various aspects have been investigated, including the existence of metastable solutions by Penrose,[16] the aggregation-dominated regime by Carr,[17] and the difficulties in numerically solving metastable systems by Carr et al.[18] and Duncan and Soheili.[19]

2.2. Generalization of the Becker−Döring Model: Catalysis. The Becker−Döring model describes general stepwise nucleation and has found applications in self-replicating systems, namely micelle and vesicle formation from a pre-curser.[6,20] Additional applications include transitional aggregation kinetics,[21] the role of chemical inhibitors in secondary nucleation,[22] monomer−monomer catalysis,[23] and dimer (two-particle clusters) interactions.[24] In ways similar to these applications, we adapt the Becker−Döring scheme to a particular situation while retaining the basic structure of the model (eqs 3 and 4).

Presently we describe the fundamental concepts of the model to be analyzed, which will be formalized later. The difficulties in modeling this system should not be underestimated. While the experimental evidence reveals the matrix effect, the mechanism by which this phenomenon occurs is entirely unknown, and hence, the model proposed below has some degree of uncertainty in the assumptions used. Previous models of vesicle formation from a precursor exhibit autocatalysis,[6] which causes vesicles to spontaneously grow at an accelerated rate after a given phase lag; the phase lag is eliminated in the presence of pre-added vesicles. The mechanism responsible for this behavior is the hydrolysis of the precursor within the vesicles, thus increasing the stock of monomers from which the vesicles grow. However, this is not sufficient to explain the size-templating matrix effect we aim to explain here, where, in the case of monodisperse pre-added vesicles, the final size distribution is biased toward the size of the pre-added vesicles. In the spirit of more recent experiments, we model the growth of vesicles from a stock of monomers, assuming that vesicles grow via two mechanisms as described by Berclaz.[11] First, there is the de novo process, where vesicles grow solely via monomer−cluster interactions and second, a more complicated monomer−cluster−cluster interaction. In the presence of a vesicle, a secondary vesicle can grow relatively rapidly (compared with de novo growth) and via a fission mechanism these disengage to form two vesicles. We propose that existing vesicles provide a catalytic surface to accelerate the assembly of vesicles; thus, a fragment of a vesicle can grow on the surface of a preexisting vesicle to form a quadruple layer. Once a fragment has started to grow, the host vesicle remains inert, and any available monomers are absorbed by the fragment as this will have comparably high reactive edges. Berclaz et al.[11] report that the majority of vesicles formed were unilamellar; the average lamellarity degree was around 1.02. Thus, we assume that the quadruple layers can undergo a fission process, and because of the nature of the matrix effect observed we assume that the fission process is heavily biased toward producing two vesicles of equal size.

The stepwise nature of the Becker−Döring model is commonly used when the concentrations of large vesicles are small and the monomer concentration is high. A more general model would take a Smoluchowski[14] form, but this greatly complicates the model. However, Chiruvolu et al.[26] report that in the particular case of mixed cationic (cetyltrimethylammonium) and anionic (sodium dodecylbenzenesulfonate) surfactant, the electrostatic repulsion between vesicles is sufficient to make the net interaction repulsive at all separations. From this we conclude that, in this case at least, monomer interactions will dominate the dynamics, thus implying that the Becker−Döring approximation is valid. We assume that as a fragment starts to grow it is sufficiently small that its charge is negligible and, hence, is bound to the surface of the host vesicle via other mechanisms, such as surface forces; however, as the fragment grows the build up of charge provides a mechanism for the separation of the fragment and host vesicle. In addition to the monomer interaction present in the Becker−Döring model, we include the growth of fragments on the surface of a vesicle and account for a fission process that allows a host/fragment pair to disengage to form two vesicles; we make the simplifying assumption that this only occurs when the fragment has grown to the same size as the host. Additionally, we assume that the fragment cannot exceed the host vesicle in size. We denote a host vesicle of r monomers with a fragment of k monomers by $F_{r,k}$. Thus, in addition to reaction 1, we include

$$C_r + C_1 \rightleftharpoons F_{r,1} \tag{11}$$

$$F_{r,k} + C_1 \rightleftharpoons F_{r,k+1} \tag{12}$$

$$F_{r,r} \rightleftharpoons 2C_r \tag{13}$$

The forward (reverse) reaction rates for reaction 11 are denoted by $\delta_r(\eta_r)$, for reaction 12 by $\alpha_{r,k}(\beta_{r,k})$, and for reaction 13 by $\phi_r(\psi_r)$, respectively. The first reaction, 11, represents monomers binding to the surface of a vesicle, rather than joining the bulk structure and initiating fragment growth; the second reaction, 12, describes the reversible growth of a fragment through monomer interactions while the host vesicle remains inert; the third reaction, 13, allows the fragment to disassociate from the host vesicle, resulting in two equal-sized vesicles. Modeling reactions 1 and 11−13 by using the law of mass action yields the following set of kinetic equations:

$$\dot{c}_1 = -J_1 - \sum_{r=1}^{\infty} J_r - \sum_{r=2}^{\infty} (\delta_r c_r c_1 - \eta_r f_{r,1}) - \sum_{r=2}^{\infty} \sum_{k=1}^{r-1} H_{r,k} \tag{14}$$

$$\dot{c}_r = J_{r-1} - J_r + 2\phi_r f_{r,r} - 2\psi_r c_r^2 - \delta_r c_r c_1 + \eta_r f_{r,1}, \quad r \geq 2 \tag{15}$$

$$\dot{f}_{r,1} = \delta_r c_r c_1 - \eta_r f_{r,1} - H_{r,1}, \quad r \geq 2 \tag{16}$$

$$\dot{f}_{r,k} = H_{r,k-1} - H_{r,k}, \quad 2 \leq k \leq r-1 \tag{17}$$

$$\dot{f}_{r,r} = H_{r,r-1} - \phi_r f_{r,r} + \psi_r c_r^2, \quad r \geq 2 \tag{18}$$

$$H_{r,k} = \alpha_{r,k} f_{r,k} c_1 - \beta_{r,k+1} f_{r,k+1} \tag{19}$$

$$J_r = a_r c_1 c_r - b_{r+1} c_{r+1} \tag{20}$$

where $f_{r,k}$ represents the concentration of host/vesicle pairs corresponding to $F_{r,k}$, and $H_{r,k}$ is the net flux from $f_{r,k}$ to $f_{r,k+1}$ because of reaction 12, the surface growth of the fragment. Numerical values for all parameters are given at the start of section 3.2.

For there to be a physically relevant equilibrium solution which satisfies a detailed balancing condition (J_r, $H_{r,k} = 0$ for all r, k), all reactions must be reversible. In eq 18 we wish the aggregation of two vesicles to be much smaller than the break up of $F_{r,r}$ into $2C_r$, and so we choose $\psi_r = A\phi_r$, with A small. In terms of the global equilibrium constant, Q_r, we aim for an equilibrium solution of the form

$$\bar{c}_r = Q_r \bar{c}_1^r, \qquad \bar{f}_{r,k} = AQ_rQ_k\bar{c}_1^{r+k} \tag{21}$$

and because A is small, at equilibrium there will be few

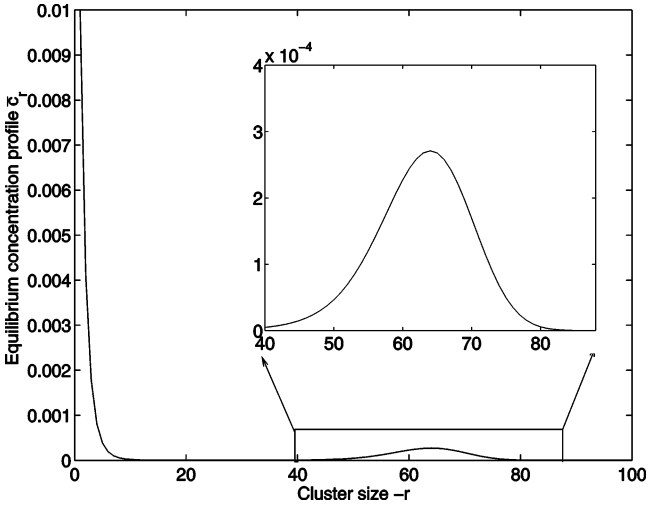

Figure 1. Plot of a typical equilibrium solution for vesicles unencumbered by fragments, that is, $\bar{c}_r$. The peak around $\bar{c}_1$ is due to small clusters being unstable. However, once clusters grow they become relatively stable and form an equilibrium peak at larger cluster sizes, the shape of which is modeled on experimental observations. Approximately 90% of the mass is centered about the peak at $r = 64$.

complexes present. An intuitive interpretation of the parameter A can be gained by rearranging eq 21 to give

$$A = \frac{\bar{f}_{r,k}}{\bar{c}_r \bar{c}_k} \tag{22}$$

For the equilibrium in eq 21 to be consistent, we chose the aggregation and fragmentation rates for the fragments to be proportional to those of the vesicle; that is, $\alpha_{r,k} = \gamma a_k$ and $\beta_{r,k+1} = \gamma b_{k+1}$. We assume that the rate at which monomers aggregate directly into vesicles is limited only by their rate of diffusion; thus, the de novo aggregation coefficient is size independent. Without loss of generality, we assume $a_r = \epsilon$, where ϵ is small ($\epsilon \ll 1$), to model relatively slow de novo growth. Thus, a choice of the equilibrium solution, via the global equilibrium constant, will define the fragmentation coefficients $b_{r+1} = \epsilon Q_r/Q_{r+1}$; this assumes that a dynamic equilibrium solution exists for the vesicles in which vesicles are continually exchanging monomers with the solution. This is a well-accepted assumption in transition-state theories. Our aim is to understand the kinetics far from equilibrium. We ensure that $\gamma\epsilon \approx \mathcal{O}(1)$, hence the fragments $F_{r,k}$ grow at an accelerated rate compared to the vesicles C_r. Finally, for the formation of fragments $F_{r,1}$ from complete vesicles C_r to be consistent with the above, we choose $\eta_r = \delta_r/A$.

To ensure an equilibrium solution in agreement with the experimental results, we choose the global equilibrium constant to have the following form:

$$Q_r = \exp(\Theta r^3 + \Pi r^2 + \Omega r - \Theta - \Pi - \Omega) \tag{23}$$

and we define Θ, Π, and Ω to give an equilibrium solution $\bar{c}_r$ as shown in Figure 1. Smaller clusters, unable to form closed spherical bilayers remain unstable; hence they peak at $\bar{c}_1$. Once the cluster grows beyond a given size they are relatively stable structures and they form a second peak at larger clusters sizes.

For simplicity and lacking any experimental evidence to the contrary, we take the following parameters to be r independent: $\phi_r = \phi$ and $\delta_r = \delta$; hence, it also follows that $\psi_r = \phi/A$ and $\eta_r = \delta/A$. A drawback of this model is that two vesicles can combine to form a host/fragment pair, which is unphysical because of the electrostatic repulsion between vesicles; however, if we insist that reaction 13 is irreversible, then an equilibrium solution satisfying a detailed balancing condition does not exist. To minimize this occurrence, we insist that $A \ll 1$.

It is only fair to mention a weakness of the derived model. We have assumed that only vesicles are formed from the surfactant; however, other structures have been observed, for example, micelles, rods, or disks. It is possible to construct a model to include transformations to these different structures, at the expense of greatly complicating the model, but the experimental results make no mention of such structures and therefore we assume their frequency is small enough to ignore.

Having derived the model and refined some of the parameters, we proceed to demonstrate its validity via a series of numerical simulations which compare favorably with the experiments. We note that this is a microscopic model, not a molecular-level model. That is, our size variable r is not counting molecules of surfactant monomer but is at a coarser level. The size of the most probable vesicles is typically of the order of 10^4-10^5 monomers, which here is reproduced as $R = 64$, and so each unit in r space corresponds to the addition of between 100 and 1000 monomer units. We envisage the monomer units aggregating individually but only consider a cluster to have grown when a sufficient number of monomer units have aggregated. This is calculated from a vesicle diameter of $D = 100$ nm and a headgroup surface area of $\sigma < 1$ nm^2, giving a typical aggregation number of $2\pi D^2/\sigma \approx 10^4-10^5$.

3. Numerical Modeling

3.1. Simplification. To numerically integrate the model, we must limit the maximum size of the system, $r_{max} = N$, allowing monomers to aggregate with c_N and therefore form a larger cluster outside the system but not to fragment from c_{N+1}. Thus, we allow mass to leave the system. More explicitly, we solve

$$\dot{c}_1 = -J_1 - \sum_{r=1}^{N} J_r - \sum_{r=2}^{N}(\delta c_r c_1 - \eta f_{r,1}) - \sum_{r=2}^{N}\sum_{k=1}^{r-1} H_{r,k} \tag{24}$$

$$\dot{c}_r = J_{r-1} - J_r + 2\phi f_{r,r} - 2\psi c_r^2 - \delta c_r c_1 + \eta f_{r,1}, \quad 2 \le r \le N \tag{25}$$

$$J_r = \epsilon\left(c_1 c_r - \frac{Q_r}{Q_{r+1}} c_{r+1}\right), \quad 1 \le r \le N-1 \tag{26}$$

$$J_N = \epsilon c_1 c_N \tag{27}$$

The equations governing the fragment growth remain unchanged 16−19, and we choose $N = 100$. The mass, ρ, is no longer conserved, but rather:

$$\dot{\rho} = -NJ_N \tag{28}$$

However, because we expect $c_N < \bar{c}_N$ and $\bar{c}_N \ll 1$ then $\dot{\rho}$ will be very small, that is, the actual amount of mass lost from the system is negligible. Thus, our results are indistinguishable from the constant mass truncation obtained by putting $a_r = 0$ for $r \ge N$. Using the equilibrium solution, we calculate the required initial mass in the system:

$$\rho = \sum_{r=1}^{N}(rQ_r\bar{c}_1^r + \sum_{k=1}^{r}(r+k)Q_rQ_k\bar{c}_1^{r+k}) \tag{29}$$

In general, we assume that at $t = 0$ all of this mass is in c_1, that

is, the initial condition $c_1(0) = \rho$ and $c_r(0) = 0$ for all $r \geq 2$. If we add some vesicles initially, the concentration of monomers is held constant and additional mass is added to the system to be consistent with the experiments. With these modeling assumptions in place we are free to consider the problem of numerically integrating the system.

3.2. Numerical Results. The numerical simulation of the model presented in the previous section requires some care in the choice of parameter values. To determine the constants Θ, Π, and Ω in Q_r (eq 23), we use the following conditions: the main peak of the equilibrium was located at $r = 64$, the minimum at $r = 25$, the ratio $\bar{c}_{64}/\bar{c}_{25} = 800$, and the equilibrium monomer concentration $\bar{c}_1 = 0.01$. This completely defines the equilibrium solution as shown in Figure 1. While the concentration of the monomers is higher than the main peak at $r = 64$, in fact, approximately 90% of the mass is in the range $25 < r$. We chose $\epsilon = 0.1$ and $\gamma = 5000$ to ensure that fragment growth dominates the de novo growth of vesicles. To minimize the aggregation of two clusters forming a fragment/host pair we set $A = 0.1$. We envisage that once a fragment has grown to the size of the host vesicle it will fragment rapidly, and therefore we assume that $\phi = 10$. To encourage fragment growth we set $\delta = 10$, so that monomers readily bind to the surface of a vesicle to initiate fragment growth. However, because $\eta_r = \delta/A$, this state is highly unstable to the break-off of the fragment, and although we expect the fragment growth to have a large impact on the dynamics, a majority of the mass will be in the C_r state. For the remainder of this paper we use the parameter values as above which, via eq 29, gives an initial mass of 0.2052.

Initially the system consists of a large number of monomers, and we find that the early dynamics, where small clusters are formed in relatively high concentrations, are typically very fast. To accurately describe this requires a small timestep, but as the system approaches equilibrium the dynamics slow drastically and therefore such a small timestep is inappropriate. Therefore, this problem naturally lends itself to a numerical scheme with an adaptive time step. We chose the NAG routine D02CJF[27] to numerically integrate the system.

To display all the data produced by the numerical simulations requires complicated 3-D graphs which confuse the essential features. Hence, we construct a distribution, e_r, which represents the size distribution which would be observed by experiment. Specifically,

$$e_r = c_r + \sum_{k=1}^{r} f_{r,k} \tag{30}$$

so that a host/fragment pair contributes only the host vesicles size to the distribution. We note that in general we found $c_r \gg f_{r,k}$ for all r and k, so that $e_r \approx c_r$.

Initially, we consider the case where mass is pre-added at $r = 55$ and the number ratio of pre-added vesicles mass to monomer mass is 1:10, that is, $c_1(0)/55c_{55}(0) = 10$ with $c_r(0) = 0$ for $r \neq 1, 55$. We find two phases of dynamics. At the outset there is a fast phase where the combination of plentiful monomers, the presence of large vesicles, and the rate of fragment initiation being larger than the de novo growth ($\delta = 10 \gg \epsilon = 0.1$) causes fragments to grow rapidly and produce vesicles of the same size as the pre-added vesicles. After this fast phase, the monomer concentration is greatly reduced and near its equilibrium value, and the growth of fragments is limited; the dynamics thus rely on the slower de novo growth. The two phases of dynamics are demonstrated in Figure 2 where the concentration profile e_r is plotted at various times.

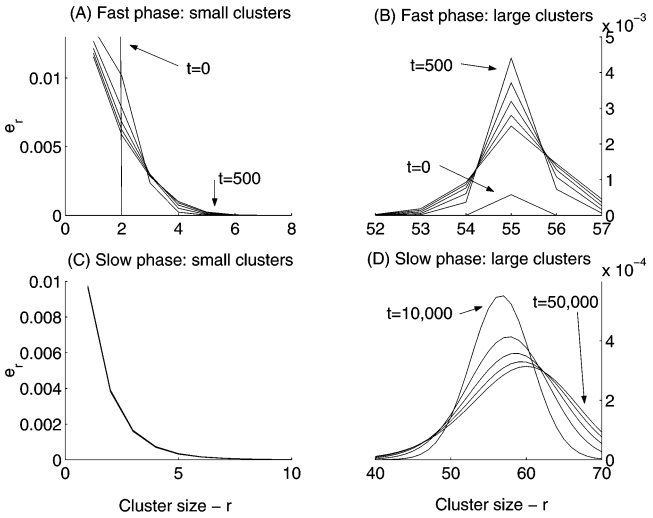

Figure 2. Pre-added vesicles were initially inserted at $r = 55$, with initial conditions $c_1(0) = \rho = 0.2052$, $c_{55}(0) = \rho/550$, $c_r(0) = 0$ for all $r \neq 1, 55$. We observe rapid aggregation to the pre-added cluster size and then slower dynamics as the system relaxes to the global equilibrium. Plots A and B show the small and large cluster sizes, respectively, in the fast phase at times 0 to 500, whereas plots C and D show the small and large cluster sizes in the slow phase, times 10 000 to 50 000. We note that the large cluster size concentration grows rapidly in the fast phase but in the slow phase falls as the distribution tends to equilibrium.

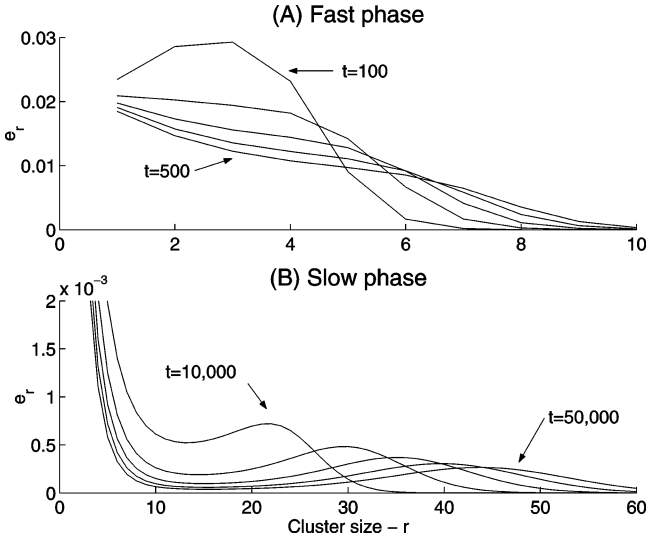

Figure 3. In this case, no pre-added vesicles were present initially, and thus, $c_1(0) = \rho$, $c_r(0) = 0$ for all $r > 2$. We plot the concentrations e_r over two timescales. (A) Plot of the small cluster concentrations from time 0−500 in steps of 100. Over the fast phase the small clusters ($r < 25$) tend to a local equilibrium. This is maintained over the slow phase but is reduced toward the global equilibrium. (B), Concentration profile plotted for large clusters over the time range 0−50 000 in steps of 10 000. Over the slow phase, mass aggregates to larger cluster sizes ($r > 25$) form a "wave" which moves toward the equilibrium peak at $r = 64$.

Next we consider the case of no pre-added vesicles, that is $c_1(0) = \rho$, $c_r(0) = 0$ for all $r \geq 2$ so that the dynamics are more reliant on the de novo process of aggregation. Figure 3 shows the concentration profile e_r at various times. Again, two phases of dynamics are identified. First, the small clusters form a local equilibrium over the range $r < 25$. Over a longer timescale, mass aggregates to larger cluster sizes and forms a "wave", which moves to larger cluster sizes and tends toward the equilibrium peak at $r = 64$; meanwhile, the smaller cluster

concentrations remain in a local equilibrium but gradually reduce to their global equilibrium values. We note that the end of the fast phase for the case without pre-added vesicles corresponds to a time at which the system with pre-added vesicles has already entered the slow phase and the concentration profile shows the characteristic peak around the pre-added cluster size. That is, the fast phase with no pre-added vesicles is not as fast as the fast phase with pre-added vesicles. This we claim to be the essential feature of the size-templating matrix effect.

3.3. Turbidity Measurements. Since turbidity is easily measured, it has been measured extensively in the experiments and can be defined as being proportional to the amount of light scattered or absorbed by the sample, rather than transmitted in straight lines through the sample. This is influenced not only by the number of particles but also by their volume. Berclaz et al.[11] note that for vesicles, volume effects have an overwhelming statistical weight in turbidity measurements. Furthermore, Berclaz et al.[10] state that it is the second power of the volume that influences turbidity. Hence, we take turbidity to be the ratio of the second and first moments of the concentrations e_r. That is,

$$\text{turbidity} = \frac{\sum_{r=1}^{N} r^2 e_r}{\sum_{r=1}^{N} r e_r} \tag{31}$$

where $M_2 = \sum_{r=1}^{N} r^2 e_r$ and $M_1 = \sum_{r=1}^{N} r e_r$. Using this definition of turbidity, we now compare our numerical simulations with the experimental data.

First, we compare systems with pre-added vesicles with varying size. Experimentally, Lonchin et al.[9] mixed a solution of 0.2 mL of 50 nM sodium oleate in water with 0.8 mL of 0.125 mM POPC vesicles suspension, so that [oleate acid + oleate]/[POPC] = 100:1; the pre-added POPC vesicles were of size 50, 100, and 200 nm in diameter. The effect on the turbidity of pre-adding these different sized vesicles is reproduced in Figure 4. Essentially, the larger the pre-added vesicles, the greater the final turbidity and the longer it takes to reach this plateau. The diameter of a vesicle is proportional to the root of the aggregation number, and thus to mimic the experiment, we compare three systems with pre-added vesicles at $r = 4$, 16, and 64. The results are shown in Figure 5. First, if we consider the case of a system with pre-added vesicles at $r = 64$ we clearly see the fast phase over the timescale $0 < t < 4$ where the turbidity rises rapidly, after which the dynamics apparently halt because the slow phase is far longer than the fast phase. Comparing the three pre-added systems, we observe that the larger the pre-added vesicles the higher the turbidity plateau reached at the end of the fast phase because the catalytic effect accelerates the growth of fragments to the same size as the pre-added vesicles. Additionally, we note that the larger the pre-added vesicles the longer the fast phase persists. Comparing the numerical results in Figure 5 with the experimental results reproduced in Figure 4, we claim that the qualitative agreement is good.

We progress to comparing systems with pre-added vesicles to those without. Consider the experiment by Berclaz et al.,[10] shown in Figure 6. This experiment compares the difference between a system with pre-added vesicles and two systems without, but with different monomer densities. More precisely, 240 μL of either 30 or 15 mM of aqueous sodium oleate solution was added to 960 μL of borate buffer, representing initial

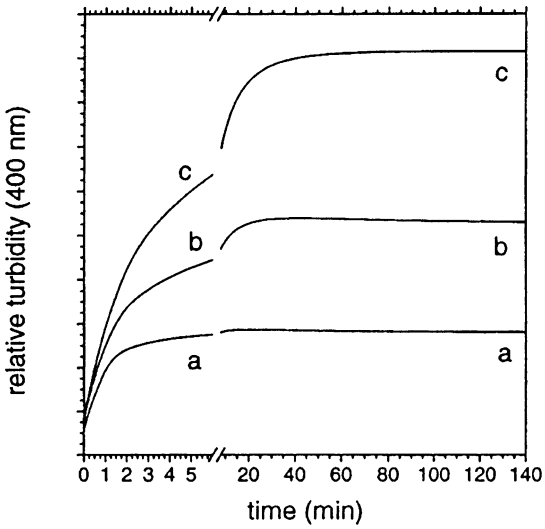

Figure 4. Effect of the size of pre-added POPC vesicles on the kinetics of mixed oleate acid/oleate/POPC vesicle formation. A solution of 0.2 mL of 50 nM sodium oleate in water was added to 0.8 mL of a 0.125 mM POPC vesicle suspension so that [oleate acid + oleate]/[POPC] = 100:1, where the pre-added POPC vesicles were (a) 50 nm, (b) 100 nm, and (c) 200 nm in diameter. Essentially, the larger the pre-added vesicles, the higher the turbidity plateau and the more time required to reach this state. Figure reproduced with permission of the author.[9]

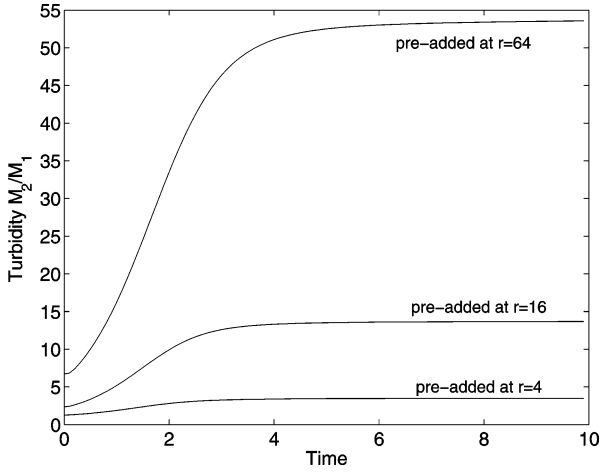

Figure 5. Numerical simulations of a system with pre-added vesicles at $r = n$, with initial conditions $c_1(0) = \rho = 0.2052$, $c_n(0) = \rho/100n$, and $c_r(0) = 0$ for all $r \neq 1$, n with $n = 4$, $n = 16$, and $n = 64$. The mass of pre-added vesicles was chosen to be 1/10 of the mass of the monomer concentration. Compare this graph with the experimental results reproduced in Figure 4.

conditions $c_1(0) = \rho$, $c_r(0) = 0$ for all $r \geq 2$ and $c_1(0) = 2\rho$, $c_r(0) = 0$ for all $r \geq 2$. These were compared with mixing 240 μL of 15 mM of aqueous sodium oleate solution to 960 μL of 3.75 mM POPC vesicles of size 100 nm; [oleate acid + oleate]/[POPC] = 1:1. The presence of the pre-added vesicles gives rise to the characteristic plateau in the turbidity, reached after a comparatively short fast phase, whereas the two systems without pre-added vesicles exhibit much slower dynamics; however, the system with twice the initial monomer mass persistently has a higher turbidity. Simulating the experiment, we numerically integrate three systems; initial conditions 1: $c_1(0) = \rho$, $c_r(0) = 0$ for all $r \geq 2$, initial conditions 2: $c_1(0) = 2\rho$, $c_r(0) = 0$ for all $r \geq 2$, initial conditions 3: $c_1(0) = \rho$, $c_{55}(0) = \rho/10$, $c_r(0) = 0$ for all $r \neq 1, 55$. The first two initial conditions correspond to systems without pre-added vesicles, with initial monomer mass ρ and 2ρ, respectively. In the final system we pre-add vesicles at $r = 55$, with concentration $\rho/10$

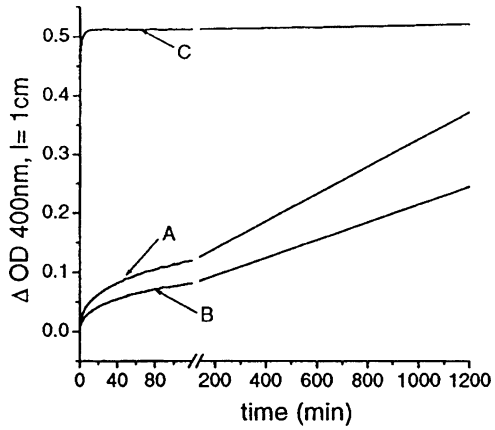

Figure 6. Graph of turbidity against time comparing two experimental systems without pre-added vesicles, but with different masses, and one with pre-added vesicles. Either 30 or 15 mM aqueous sodium oleate solution was added to 960 μL of borate buffer, thus representing initial conditions $c_1(0) = \rho$, $c_r(0) = 0$ for all $r \geq 2$ (curve B) and $c_1(0) = 2\rho$, $c_r(0) = 0$ for all $r \geq 2$ (curve A). These were compared with mixing 240 μL of 15 mM aqueous sodium oleate solution to 960 μL of 3.75 mM POPC vesicles of size 100 nm; [oleate acid + oleate]/[POPC] = 1:1 (curve C). We note that the system without pre-added vesicles, but with $c_1(0) = 2\rho$, maintains a higher turbidity than the system with mass ρ. Additionally, the fast dynamics of the system with pre-added vesicles is almost unobservable over the timescale of the system without pre-added vesicles. Figure reproduced with permission of the author.[10]

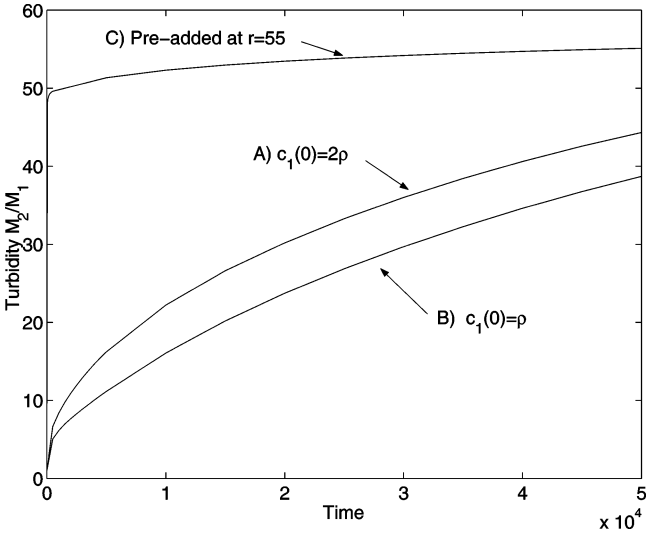

Figure 7. We estimate turbidity by M_2/M_1 for the concentrations e_r for three systems to compare with the experimental results reproduced in Figure 6. (A) No pre-added vesicles with initial conditions $c_1(0) = 2\rho$, $c_r(0) = 0$ for all $r > 2$. (B) No pre-added vesicles but with half the monomer mass compared with the previous case; initial conditions $c_1(0) = \rho$, $c_r(0) = 0$ for all $r > 2$. (C) Pre-added vesicles at $r = 55$ with initial conditions $c_1(0) = \rho$, $c_{55} = \rho/10$, $c_r(0) = 0$ otherwise. We note that the qualitative agreement with the experimental data is good.

so the total mass is $(1 + 55/10)\rho$. Figure 7 compares the turbidity of these systems. First, we note that the timescale for the systems without pre-added vesicles is sufficiently long that the fast phase of the system with pre-added vesicles is not apparent, as is the case with the experimental data. Considering initial conditions 1, we observe that after a relatively rapid rise the turbidity increases at a more moderate, but sustained, rate. The qualitative agreement with the experimental data reproduced in Figure 6 is good; with no pre-added vesicles, doubling the initial monomer mass leads to a higher turbidity over the entire time range.

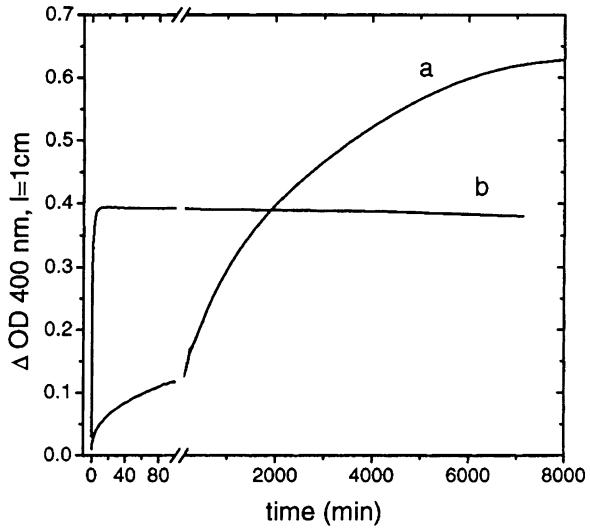

Figure 8. Graph of turbidity against time comparing two experimental systems: with and without pre-added vesicles. A solution of 0.2 mL of 25 mM sodium oleate in water was added to either (a) 0.8 mL of 0.1 M borate buffer solution, pH 8.5 or (b) 0.8 mL of 0.25 mM POPC vesicle suspension (100 nm in diameter), pH 8.5. The shape of the curves is described in the experiments reproduced earlier; however, here we observe that the system without pre-added vesicles eventually reaches a turbidity far in excess of the plateau obtained by the system with pre-added vesicles. Figure reproduced with permission of the author.[11]

More direct comparison between systems with and without pre-added vesicles has yielded some intriguing results. Berclaz et al.[11] used turbidity to determine the effect of the presence of preformed 100 nm POPC vesicles on the kinetics of mixed oleic acid/oleate/POPC vesicles. The results are reproduced in Figure 8. The form of each curve is as previously described, but the plateau that the pre-added system reaches is far exceeded by the case without pre-added vesicles. With our approximation for turbidity (eq 31), this is a phenomena we have been unable to reproduce. However, more detailed experiments using cryotransmission electron microscopy confirm the view that the higher turbidity of the system without pre-added vesicles is due to a broader distribution of sizes. With this in mind, we examine in Figure 9 the distribution, e_r, at $t = 100\,000$ for initial conditions 1 (without pre-added vesicles) and 3 (with pre-added vesicles) in the previous numerical simulation.

We measure the standard deviation of the concentration distribution from the first minimum point to the largest cluster size, $r_{min} < r < 100$, and find that with pre-added vesicles the standard deviation is 7.56 and without pre-added vesicles the standard deviation is 11.03. Hence, we also observe a broader distribution in the case of no pre-added vesicles; however, we concede that the effect reported experimentally was far more striking.

In summary, we have developed a detailed microscopic model of vesicle formation which incorporates the catalytic mechanism of fragments growing on the surface of a vesicle. This model is then approximated to permit numerical simulation, and we have demonstrated the validity of the model by qualitatively reproducing experimental results, mainly via an estimate of the turbidity of the system.

4. Conclusion

We have constructed a microscopic model of the formation of vesicles, from an initial stock of surfactant, based on a generalization of the Becker−Döring model of nucleation. The

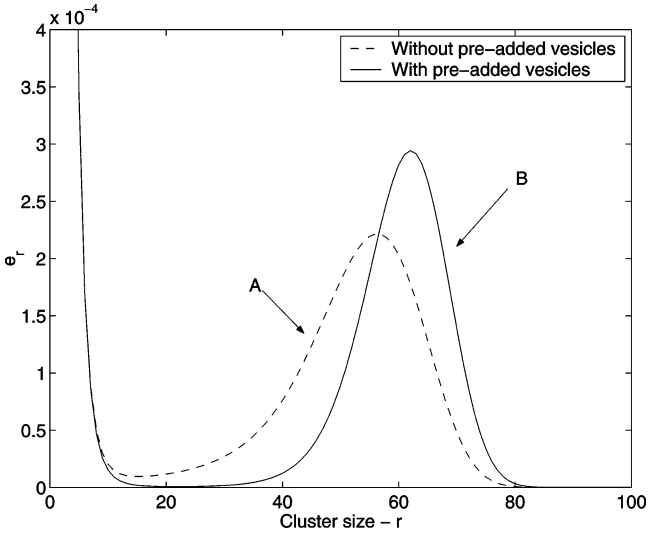

Figure 9. Concentration e_r for two systems at $t = 100\,000$. (A) No pre-added vesicles, with initial conditions $c_1(0) = \rho$, $c_r(0) = 0$ for all $r > 2$. (B) With pre-added vesicles at $r = 55$, with initial conditions $c_1(0) = \rho$, $c_{55}(0) = \rho/10$, $c_r(0) = 0$ otherwise. We measure the standard deviation form the first minimum point to the largest cluster size, $r_{min} < r < 100$. Plot A has a standard deviation of 11.03, whereas B has a standard deviation of 7.56. Thus, the case with pre-added vesicles has a narrower distribution.

central assumption of the model analyzed is that clusters grow in a stepwise fashion, that is, only a monomer may aggregate, or fragment, from a cluster at any single nucleation event. While rate constants have been derived by assuming the existence of an equilibrium size distribution of vesicles, all our simulations and observed phenomena occur away from equilibrium and the timescales for convergence to equilibrium are extremely long. By altering the Becker−Döring model we include a surface catalytic effect, where a fragment of a vesicle can grow on the surface of a preexisting vesicle and eventually disengage the host vesicle to result in two complete and separate vesicles. Experimentally it has been observed that the presence of pre-added vesicles of a particular size influences the final distribution of vesicles, which is biased toward the size of the pre-added vesicles, and accelerates the dynamics. Thus, we assume that a fragment only leaves the host vesicle when it grows to the same size. In experiments, tagging the pre-added vesicles with ferritin has established that the mechanism of growth introduced by the presence of pre-added vesicles dominates the de novo formation process. Thus, we assume that the fragment growth rate, while having the same size dependence as the de novo growth rate, is accelerated.

In modeling vesicle growth, we have chosen the forms of various parameters. We used size-independent aggregation rates and size-dependent fragmentation rates to ensure that the system tends to a predetermined equilibrium. Although the probability of fragments initiating on a vesicle was high, in equilibrium the numbers of fragments were very low. We chose the probability of a fully grown fragment disengaging a host vesicle to be high compared with the probability of two vesicles forming a fragment/host complex; for simplicity these and the remaining parameters were deemed to be size independent.

We numerically integrated a truncated version of the model for a particular set of parameters to investigate the types of behavior possible. In the presence of pre-added vesicles, two phases of dynamics were found. Initially a fast phase, during which a majority of mass in the system aggregated to the size of the pre-added vesicles, which is followed by a distinct slow phase where the system relaxes toward a global equilibrium. During the fast phase, the dynamics are dominated by the growth of vesicle fragments on the surface of preexisting vesicles, thus manufacturing more vesicles of the same size. Over the slow phase the lack of monomers inhibits the fragment growth, and the dynamics are dominated by the absorption of monomers into vesicles without fragments, causing growth in the size of vesicles and a broadening in vesicle-size distribution. We postulate that the end of the fast phase corresponds to the experimentally observed results, so that the size of the pre-added vesicles has strongly biased the final distribution. In the case without pre-added vesicles, we identified a slower fast phase over which a local equilibrium is reached for the small-sized vesicles ($r < 25$). The system then makes a more gradual transition to the slower phase behavior as mass aggregates toward larger cluster sizes as the system tends to the global equilibrium. Our model contains several rate-determining parameters: ϵ controls the growth rate of vesicles by absorption from solution and is small, δ controls the rate at which new fragments are nucleated on the surface of a preexisting vesicle, γ controls the growth rate of fragments, ϕ controls the release rate of fragments from the host vesicles, and A controls the proportion of fragments on vesicles at equilibrium and is also small. Thus, ϵ determines the kinetics in the slow phase and γ determines the kinetics of the fast phase, with δ, ϕ, and A also playing a role in the kinetics of the fast phase.

Approximating the turbidity by the ratio of the second to the first moment of the size distribution (M_2/M_1), we were able to compare the model with three sets of experimental results. First, Lonchin et al.[9] compares the effect of pre-adding a hundredth of the mass of monomers as vesicles of a particular cluster size. The larger the pre-added vesicles, the greater the final turbidity and the greater the time to reach this state. Second, Berclaz et al.[10] compares two systems of different masses without pre-added vesicles with one with pre-added vesicles. The pre-added case has the typical fast phase of dynamics followed by very slow dynamics, whereas the turbidity of the two systems without pre-added vesicles are approximately proportional to the mass. For both experiments we have demonstrated that our model qualitatively captures the experimental results, thus validating the model. Finally, we considered an experiment by Berclaz et al.[11] where a system with pre-added vesicles is compared to one without. The final turbidity of the system without pre-added vesicles was found to be higher than the system with pre-added vesicles. While not being able to reproduce this result, we argue that M_2/M_1 is only an approximation to turbidity and that the "final" concentration profile, e_r after 10^5 nondimensional time units, of the numerical results shows that the standard deviation for the case with pre-added vesicles is smaller than that without pre-added vesicles, which is in agreement with more detailed cryotransmission electron microscopy measurements.

The complexity of the model does not permit an analytical solution to be found, and therefore we relied on numerical methods. However, this can only illuminate the dynamics for particular chosen parameters, which in turn can only demonstrate the types of behavior possible with this model. We have reduced this microscopic model to a low-order system of ordinary differential equations by a course-graining approach, which is more analytically tractable and will be described and analyzed in a future paper.[25]

Acknowledgment. Colin Bolton is supported by an EPSCRC studentship. We wish to thank P. L. Luisi for allowing us to reproduce Figures 4, 6, and 8. Our thanks also go to the

reviewers for providing helpful suggestions in improving the clarity of the manuscript.

References and Notes

(1) Dyson, F. J. *Origins of Life*; Cambridge University Press: New York, 1985.
(2) Oró, J.; Miller, S. L.; Lazcano, A. *Annu. Rev. Earth Planet. Sci.* **1990**, *18*, 317.
(3) Walde, P.; Wick, R.; Fresta, M.; Mangone, A.; Luisi, P. L. *J. Am. Chem. Soc.* **1994**, *116*, 11649.
(4) Blöchliger, E.; Blocher, M.; Walde, P.; Luisi, P. L. *J. Phys. Chem. B* **1998**, *102*, 10383.
(5) Mavelli, F.; Luisi, P. L. *J. Phys. Chem.* **1996**, *100*, 16600.
(6) Coveney, P. V.; Wattis, J. A. D. *J. Chem. Soc., Faraday Trans.* **1998**, *94*, 233.
(7) Lifson, S. *J. Mol. Evol.* **1997**, *44*, 1.
(8) Blöchliger, E.; Blocher, M.; Walde, P.; Luisi, P. L. *J. Phys. Chem. B* **1998**, *102*, 10383.
(9) Lonchin, S.; Luisi, P. L.; Walde, P.; Robinson, B. H. *J. Phys. Chem. B* **1999**, *103*, 10910.
(10) Berclaz, N.; Blöchliger, E.; Müler, M.; Luisi, P. L. *J. Phys. Chem. B* **2001**, *105*, 1065.
(11) Berclaz, N.; Müller, M.; Walde, P.; Luisi, P. L. *J. Phys. Chem. B* **2001**, *105*, 1056.
(12) Becker, R.; Döring, W. *Ann. Phys.* **1935**, *24*, 719.
(13) Penrose, O.; Lebowitz, J. L. *Studies in Statistical Mechanics VII: Fluctuation Phenomena*; North-Holland: Amsterdam, 1976.
(14) von Smoluchowski, M. *Phys. Z.* **1916**, *17*, 557.
(15) King, J. R.; Wattis, J. A. D. *J. Phys. A: Math. Gen.* **2002**, *35*, 1357.
(16) Penrose, O. *Commun. Math. Phys.* **1989**, *124*, 515.
(17) Carr, J.; Dunwell, R. M. *Proc. Edin. Math. Soc.* **1999**, *42*, 415.
(18) Carr, J.; Duncan, D. B.; Walshaw, C. H. *IMA J. Numer. Anal.* **1995**, *15*, 505.
(19) Duncan, D. B.; Soheili, A. R. *Appl. Num. Math.* **2001**, *37*, 1.
(20) Coveney, P. V.; Wattis, J. A. D. *Proc. R. Soc. London, Ser. A* **1996**, *452*, 2079.
(21) Krapivsky, P. L.; Redner, S. *Phys. Rev. E* **1996**, *54*, 3553.
(22) Wattis, J. A. D.; Coveney, P. V. *J. Chem. Phys.* **1997**, *106*, 9122.
(23) Krapivsky, P. L. *Phys. Rev. E* **1995**, *52*, 3455.
(24) Bolton, C. D.; Wattis, J. A. D. *J. Phys. A: Math. Gen.* **2002**, *35*, 3183.
(25) Bolton, C. D.; Wattis, J. A. D. Unpublished work, 2002.
(26) Chiruvolu, S.; Israelachvili, J. N.; Naranjo, E.; Xu, Z.; Zasadzinski, J. A.; *Langmuir* **1995**, *11*, 4256−4266.
(27) NAG routines, Mark 19, Oxford, 1999.